analytical chemistry

pubs.acs.org/ac Letter

Cross-Reactive Fluorescent Sensor Array for Discrimination of Amyloid Beta Aggregates

Pangmiaomiao Zhang and Chunyan Tan*

Cite This: https://doi.org/10.1021/acs.analchem.2c00579 Read Online

ACCESS | Metrics & More | Article Recommendations | Supporting Information

ABSTRACT: It has been hypothesized that misfolding and misassembly of proteins into various aggregation states contribute to several neurodegenerative diseases. For instance, amyloid beta (Aβ) aggregation is considered a major factor in Alzheimer's disease pathogenesis. Herein, a fluorescent sensor array for detecting Aβ aggregates was fabricated using two probe pairs of conjugated polyelectrolytes and organic dye molecules, PPE1-Thioflavin T (ThT) and PPESO3-Nile Red (NR). Pattern recognition was achieved by linear discriminant analysis and hierarchical clustering analysis algorithms. As a result of distinguishing among monomers and three pure aggregate species, namely oligomers, protofibrils, and fibrils, the cross-reactive sensor array was also able to monitor aggregation kinetics in various aggregate forms and distinguish between on- and off- aggregate pathways. Our study provides a convenient approach for simultaneous detection of Aβ aggregates in mixtures, which may also be applied to the analysis of other disease-related proteins that are prone to aggregates.

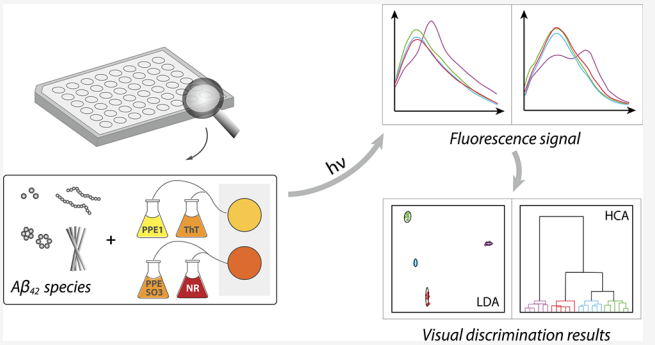

The aggregation of proteins and peptides is a hallmark of pathologies of several neurodegenerative diseases, such as Alzheimer's disease (AD), Parkinson's disease (PD), and amyotrophic lateral sclerosis (ALS).[1−4] Although the causes and effects of the aggregation of proteins and peptides on diseases have yet to be clarified extensively, the specific alloforms and aggregation states are indeed involved in the diagnosis and therapy of those conditions.[4] For example, among all the alloforms of amyloid β (Aβ) peptides, Aβ_{42} is the most toxic and aggregation-prone in the brains of AD patients.[5,6] The major aggregation states of Aβ_{42} include oligomers, protofibrils, and fibrils (Figure 1a), among which oligomers are regarded as the prominent neurotoxins for AD progression.[5,7]

There is a broad spectrum of techniques available to study protein aggregation, such as size exclusion chromatography (SEC), polyacrylamide gel electrophoresis (PAGE), mass spectroscopy (MS), analytical ultracentrifugation (AUC), and immunoassays.[4,8,9] Despite their effectiveness for determining aggregate composition, those methods are expensive and time-consuming and cannot be used for high-throughput analysis. The use of fluorescence detection allows for an alternative that is both cost-effective and specific. Small molecules like Thioflavin T (ThT), Congo Red (CR), and Nile Red (NR) bind specifically with fibril structures and respond with fluorescence change,[10,11] but they do not detect intermediates in the mixture. Several novel fluorescent probes have recently been developed to detect Aβ peptides,[10,12−15] but most of them focused on a single aggregation state or even ignored the aggregation-prone characteristic. Therefore, there has been considerable interest in developing efficient methods to detect aggregates in mixtures simultaneously, and understand aggregation kinetics and pathways.

Inspired by the human olfactory system, sensor array-based methods have emerged for high-sensitivity and broad-responsive chemical and biological sensing of mixtures with similar analytes and complex background.[16] To our knowledge, there is some research constructing sensor arrays to study Aβ aggregates.[17−20] Some used nanomaterials as the probes,[17,19,20] and one work reported a combinatorial fluorescent sensor.[18] Although those designs were carried out with high discrimination efficacy, some drawbacks exist, including complex synthesis procedures or a lack of exploring aggregation pathways and kinetics.

Herein, we present a simple cross-reactive fluorescent sensor array with two probe pairs, each consisting of both a polymer and an organic dye, PPE1-ThT and PPESO3-NR (Figure 1c; UV−visible absorption and fluorescence emission spectra of

Received: February 3, 2022
Accepted: March 30, 2022

https://doi.org/10.1021/acs.analchem.2c00579
Anal. Chem. XXXX, XXX, XXX−XXX

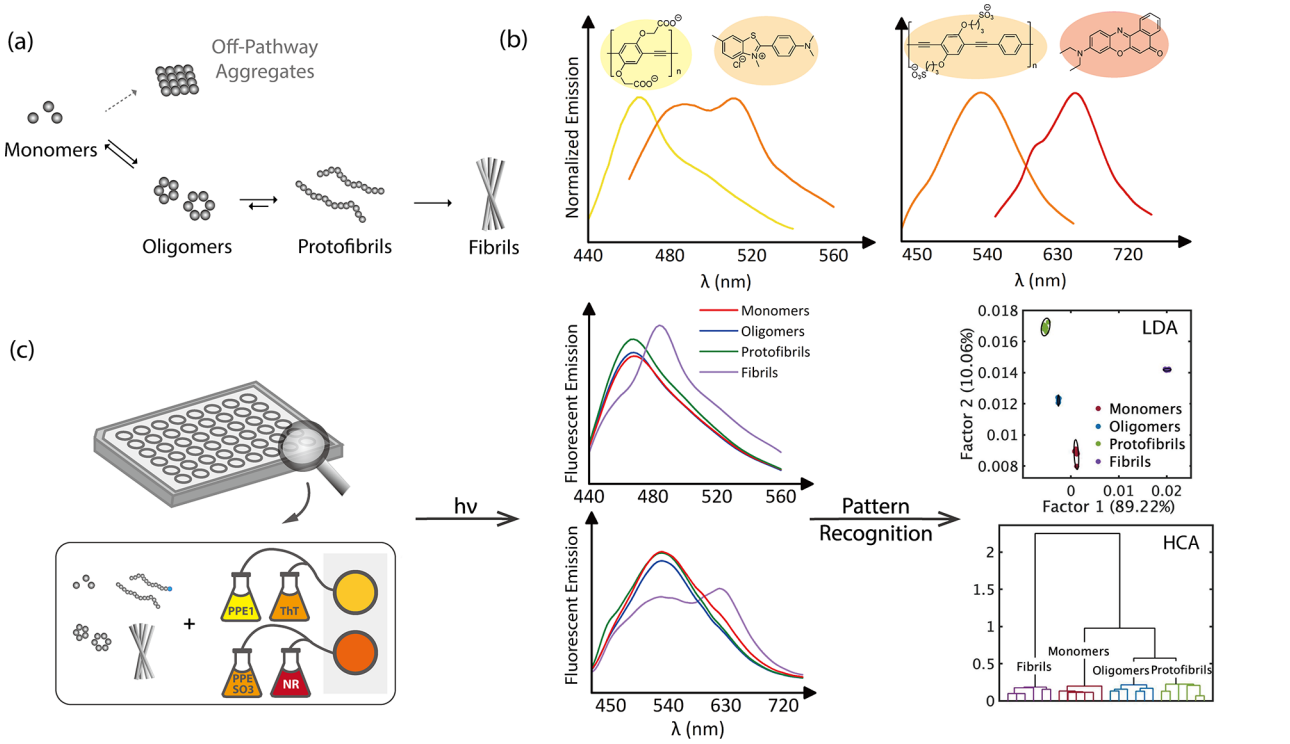

Figure 1. (a) Schematic illustration of the Aβ aggregation process and main aggregate species. (b) Normalized emission spectra of four fluorescent probes. Left, PPE1 (yellow) and ThT (orange); right, PPESO3 (orange) and NR (red). (c) Schematic diagram to show the mechanism of the cross-reactive sensor array detecting monomers and main Aβ aggregate species.

the four individual probes are shown in Figure S1). PPE1 and PPESO3 are water-soluble conjugated polyelectrolytes (CPEs) with a polymeric p-phenylene ethynylene (PPE) backbone. CPEs are sensitive to minor conformational and environmental changes, making them suitable materials for sensing proteins, DNAs, and other disease-related biomarkers.[21,22] Recent studies showed that probes with similar structures, such as oligomeric p-phenylene ethynylene (OPE) and polythiophene (PT),[23,24] caused spectral shifts in Aβ aggregates, indicating the possibility of using PPEs as array elements. Using two probe pairs rather than four probes individually allows simultaneous observations of various parameters, including changes in fluorescence intensity and spectral shifts, and produces additional dimensionality in the sensor array (Figure 1b). With this approach, we are able to produce relatively more "cross-reactive" responses for discriminating between monomers and the different aggregates of Aβ_{42}.

The proof-of-concept of the cross-reactive sensor array was verified by initially comparing fluorescence responses of the two probes pairs against the four individual probes in the differentiation of monomers and three pure representative Aβ_{42} aggregates, including oligomers, protofibrils, and fibrils. Each aggregate species was prepared according to the reported methodology (see the Supporting Information) and was characterized using transmission electron microscopy (TEM) (Figure 2a) and circular dichroism (CD) (Figure 2b). Although monomers could not be seen clearly in the TEM images because of the limited resolution, morphology demonstrates that all aggregates were virtually homogeneous. We found that the oligomers prepared at low-salt conditions are primarily small pseudospheres with an average diameter of 25−30 nm, whereas the short, narrow protofibrils have lengths over 50 nm, and the mature fibrils display extended and dense

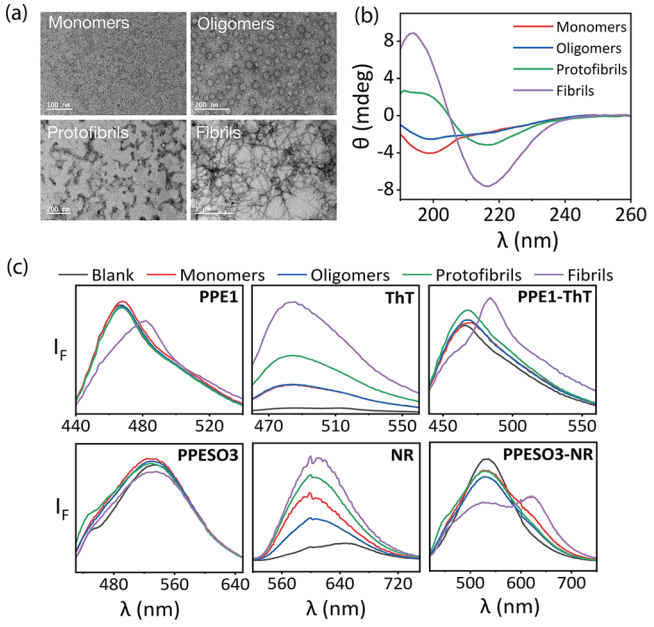

Figure 2. (a) TEM images of four pure Aβ_{42} species (40 μM). (b) CD spectra of four isolated Aβ_{42} species (16 μM). (c) Emission spectra generated by individual probes and mixed probes in response to the pure Aβ_{42} monomers and aggregate species (4 μM).

networks. CD spectra show the increasing signal at 195 nm and the decreasing signal at 218 nm, suggesting a conformational change from a random-coil to a β-sheet during the aggregation process.

The fluorescent signal was measured using a microplate reader with optimized parameters before and after the addition of Aβ_{42} peptides (Table S1). Figure 2c compares the

https://doi.org/10.1021/acs.analchem.2c00579
Anal. Chem. XXXX, XXX, XXX−XXX

fluorescence patterns produced by the four individual probes versus the two probe pairs. Different sizes, charges, side-chain functional groups, and hydrophobic properties may be responsible for the difference in fluorescent responses of the two conjugated polyelectrolytes (CPEs). As a result, there are no apparent differences in the fluorescence spectra of PPE1 upon the addition of monomers, oligomers, and protofibrils. However, the fluorescence emission peak of PPE1 shows an apparent bathochromic shift from the monomer to the fibril structure, which is consistent with the previously reported phenomenon of backbone planarization of the conjugated region upon binding to the planar site of the amyloid fibril.[23] After adding different Aβ_{42} species, the fluorescence spectra of PPESO3 are slightly altered, except for protofibrils, where the emission at 450 nm increases a little bit. As for ThT and NR, the fluorescence intensity increases continuously in response to the aggregation process as the β-sheet composition increases, while the emission peaks have no significant shift. Spectral overlap between polymers and small molecules produces a more distinct fluorescence pattern. The phenomenon could be explained by the Forster resonance energy transfer (FRET) effect between probe pairs, especially for the detection of fibrils. It has been reported in previous studies that some small organic dyes could insert into the β-sheet of high molecular weight aggregate species,[25] while the rigid backbone of CPEs could align with the fibrils.[24] As a result, FRET can be observed in the paired probes with Aβ_{42} fibrils, due to close proximity of the polymer and the dye. Both intensity changes and spectral shifts are observed, thus proving the validity of the sensor array design.

Linear discriminant analysis (LDA) and hierarchical clustering analysis (HCA) were performed using Matlab software (version R2018a) for the analysis of fluorescence patterns. Fluorescence data were preprocessed by calculating the fold-changes (I/I_0) of every point on the spectrum before analysis. For each experiment, six replicate measurements were conducted. As a result of the LDA analysis, the training data were transformed into three canonical scores, of which the two dominant ones were used to draw the two-dimensional (2-D) plot and 95% confidence ellipses. As shown in Figure 3a,c, probe pairs are significantly more effective at differentiating monomers and oligomers than the four individual probes. With more features taken into consideration when computing Euclidean distances among samples, the HCA method successfully discriminates four conformations using the four individual probes (Figure 3b) and two probe pairs (Figure 3d) without error. In addition, the LOOCV (leave-one-out cross-validation) method, which was applied to evaluate the prediction capacity, showed 100% accuracy for both methods.

Furthermore, we investigated the potential of the optimized sensor array to examine the dynamics of aggregation under various conditions. As a means of accelerating the aggregation process, different fibril seeds (0.5%, 3%, 6%) were added to the reaction. Fluorescence spectra of the probe pairs were measured at intervals until the aggregation process was completed (Figures 4b and S2). While the fluorescence spectra display a range of aggregation kinetics in terms of how fast and how extensive the aggregation is, there is a consistent pattern for all conditions. Generally speaking, the emission peak of PPE1-ThT probe pairs shifts from 470 to 485 nm; PPESO3-NR has a decrease in fluorescence signal at 520 nm and an increase at 625 nm, indicating an increasing in fibril contents over time. With a higher seed concentration, the

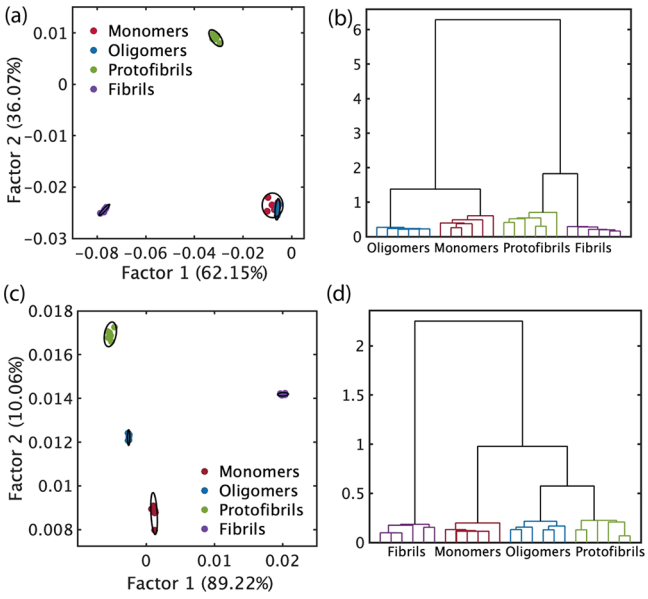

Figure 3. LDA canonical plots and HCA dendrograms for the differentiation of monomers and three pure Aβ_{42} aggregate species, including oligomers, protofibrils and fibrils (4 μM) using different sensor arrays. (a,b) Four individual probes, including PPE1, PPESO3, ThT, and NR, and (c,d) two probe pairs, PPE1-ThT and PPESO3-NR.

peptides aggregate more rapidly. TEM was used to characterize the fibril structure for all final products obtained under different conditions (Figures 4a and S3). TEM images suggest that fibril amount increases as the seed concentration increases.

To further visualize the aggregation kinetics, fluorescence patterns generated under various conditions of inducing aggregations were compared to spectra of monomers and three pure aggregate species using the LDA algorithm. According to Figure 4c, the aggregation kinetics curves exhibit variations under each of the three conditions, but they share similar patterns consistent with the emission spectra. A general pattern is apparent for the data clusters under all conditions with a trend that moves continuously from right to left, indicating a higher fibril content as the result of seed-induced aggregation. Data clusters at 0 h in all three kinetics plots are close to the pure monomer group. Although the intermediate clusters do not overlap with clusters of other pure aggregates as there was no further purification, the position of the kinetics curve indicates different compositions of aggregates under the three different conditions. Specifically, a 6% seed concentration results in more fibril-containing aggregates, while a 0.5% seed concentration results in higher protofibril concentrations and a downward kinetics curve. Furthermore, the emission intensity of PPE1-ThT at 485 nm and fibril amount displayed in TEM images at the final time point were also higher under higher seed concentrations, which confirms the results of the LDA analysis.

Chemical compounds have been reported to modulate Aβ aggregation and alter the aggregation pathway,[26−31] among which some stimulate fibril production and others inhibit fibril production, referred to as "on-pathway" and "off-pathway", respectively. As far as we know, some experimental techniques for determining secondary structures of peptides, such as CD, are limited in their ability to differentiate between fibrils and amorphous aggregates as they both exhibit a β-sheet

https://doi.org/10.1021/acs.analchem.2c00579
Anal. Chem. XXXX, XXX, XXX−XXX

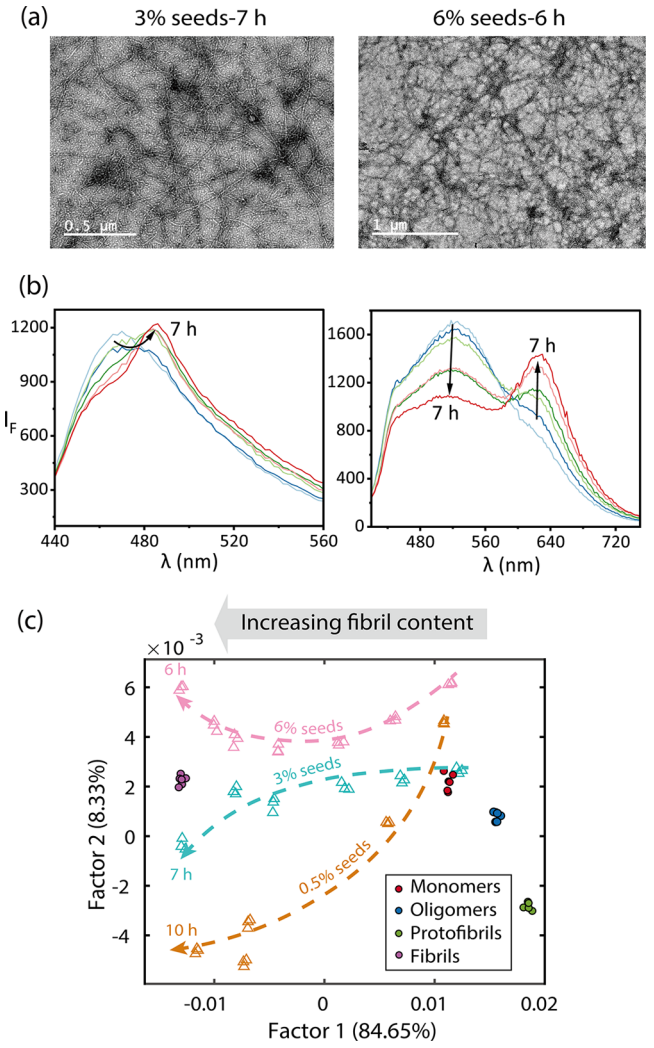

Figure 4. (a) TEM images of Aβ_{42} aggregates obtained under different conditions, including 3% seeds and 6% seeds. (b) Emission spectra of aggregation kinetics under 3% seeds. Left, PPE1-ThT; right, PPESO3-NR. (c) LDA canonical plots for the aggregation kinetics under different conditions, including 0.5% seeds, 3% seeds, and 6% seeds.

structure.[26] The array-based method provides a greater degree of spectral information and is more discriminative. In this study, six different types of stimuli were utilized to alter the aggregation pathway, including two metal ions (Cu^{2+} and Zn^{2+}), three natural chemicals (betulinic acid (BetA), capric acid (CapA), and resveratrol), and one detergent (SDS). Except for betulinic acid, which leads to fibril production, the other compounds all function "off-pathway". The fluorescence spectra of the two probe pairs were measured and analyzed using LDA algorism in response to different kinds of stimuli-induced aggregates (Figure S4). We have also confirmed the aggregation pathway using TEM (Figures 5b and S5) and CD (Figure S6). As shown in Figure 5a, the data clusters of "off-pathway" aggregates are scattered along the left side of the plot, whereas the "on-pathway" aggregates are clustered together in one category and well separated from other data points, in other words, discrimination between pathways using our two-probe pair sensor array is achieved. These results demonstrate a potential method for screening Aβ peptide aggregation inhibitors.

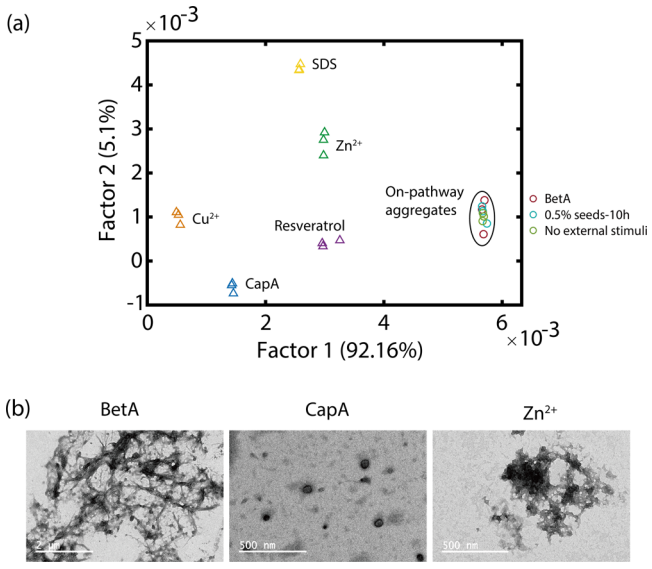

Figure 5. (a) LDA canonical plots for the discrimination of Aβ_{42} aggregates generated by different pathways. (b) TEM images of Aβ_{42} aggregates stimulated by BetA, CapA, and Zn^{2+}.

In conclusion, we have constructed a cross-reactive fluorescent sensor array using two probe pairs, PPE1-ThT and PPESO3-NR, for discrimination of Aβ_{42} monomers and different aggregate species. By using two probe pairs, we were able to achieve more cross-reactive responses and more effective discrimination as opposed to using four probes individually. In addition, the sensor array was successfully used to monitor the aggregation kinetics as well as discriminate aggregation pathways under different conditions. As our cross-reactive sensor array generates more spectral information, it provides better performance than fluorescent probes that respond to only one aggregation state, and has the potential to analyze complex mixtures and screen for active inhibitors of aggregation. This study also demonstrates a convenient and efficient approach to analyzing other diseases-related molecules that are aggregation-prone.

■ ASSOCIATED CONTENT

Supporting Information

The Supporting Information is available free of charge at https://pubs.acs.org/doi/10.1021/acs.analchem.2c00579.

Experimental details, data analysis methods, and supplementary figures of fluorescent response and characterization results (PDF)

■ AUTHOR INFORMATION

Corresponding Author

Chunyan Tan − *State Key Laboratory of Chemical Oncogenomics, Shenzhen International Graduate School, Tsinghua University, Shenzhen 518055, People's Republic of China;* orcid.org/0000-0002-4263-2175; Email: tancy@sz.tsinghua.edu.cn

Author

Pangmiaomiao Zhang − *State Key Laboratory of Chemical Oncogenomics, Shenzhen International Graduate School, Tsinghua University, Shenzhen 518055, People's Republic of China*

Complete contact information is available at:

https://doi.org/10.1021/acs.analchem.2c00579
Anal. Chem. XXXX, XXX, XXX−XXX

https://pubs.acs.org/10.1021/acs.analchem.2c00579

Notes

The authors declare no competing financial interest.

■ ACKNOWLEDGMENTS

The authors acknowledge the financial support from the State Key Laboratory of Chemical Oncogenomics and the Shenzhen Bay Laboratory Open Funding (SZBL2019062801009).

■ REFERENCES

(1) Ross, C. A.; Poirier, M. A. *Nat. Med.* **2004**, *10*, S10−17.
(2) Eisele, Y. S.; Monteiro, C.; Fearns, C.; Encalada, S. E.; Wiseman, R. L.; Powers, E. T.; Kelly, J. W. *Nat. Rev. Drug. Discovery* **2015**, *14*, 759−780.
(3) Aguzzi, A.; O'Connor, T. *Nat. Rev. Drug. Discovery* **2010**, *9*, 237−248.
(4) Pedersen, J. T.; Heegaard, N. H. *Anal. Chem.* **2013**, *85*, 4215−4227.
(5) Qiu, T.; Liu, Q.; Chen, Y. X.; Zhao, Y. F.; Li, Y. M. *J. Pept. Sci.* **2015**, *21*, 522−529.
(6) Wang, J.; Gu, B. J.; Masters, C. L.; Wang, Y. J. *Nat. Rev. Neurol.* **2017**, *13*, 612−623.
(7) Hamley, I. W. *Chem. Rev.* **2012**, *112*, 5147−5192.
(8) Ruggeri, F. S.; Šneideris, T.; Vendruscolo, M.; Knowles, T. P. J. *Arch. Biochem. Biophys.* **2019**, *664*, 134−148.
(9) Young, L. M.; Saunders, J. C.; Mahood, R. A.; Revill, C. H.; Foster, R. J.; Ashcroft, A. E.; Radford, S. E. *Methods* **2016**, *95*, 62−69.
(10) Lee, D.; Kim, S. M.; Kim, H. Y.; Kim, Y. *ACS Chem. Neurosci.* **2019**, *10*, 2647−2657.
(11) Mishra, R.; Sjolander, D.; Hammarstrom, P. *Mol. Biosyst.* **2011**, *7*, 1232−1240.
(12) Teoh, C. L.; Su, D.; Sahu, S.; Yun, S. W.; Drummond, E.; Prelli, F.; Lim, S.; Cho, S.; Ham, S.; Wisniewski, T.; Chang, Y. T. *J. Am. Chem. Soc.* **2015**, *137*, 13503−13509.
(13) Liu, B.; Shen, H.; Hao, Y.; Zhu, X.; Li, S.; Huang, Y.; Qu, P.; Xu, M. *Anal. Chem.* **2018**, *90*, 12449−12455.
(14) Zhang, X.; Tian, Y.; Zhang, C.; Tian, X.; Ross, A. W.; Moir, R. D.; Sun, H.; Tanzi, R. E.; Moore, A.; Ran, C. *Proc. Natl. Acad. Sci. U. S. A.* **2015**, *112*, 9734−9739.
(15) Zhou, Y.; Lv, Y.; Dong, H.; Liu, L.; Mao, G.; Zhang, Y.; Xu, M. *Sens. Actuators, B* **2021**, *331*, 129429.
(16) Li, Z.; Askim, J. R.; Suslick, K. S. *Chem. Rev.* **2019**, *119*, 231−292.
(17) Ghasemi, F.; Hormozi-Nezhad, M. R.; Mahmoudi, M. *Nanoscale* **2018**, *10*, 6361−6368.
(18) Hatai, J.; Motiei, L.; Margulies, D. *J. Am. Chem. Soc.* **2017**, *139*, 2136−2139.
(19) Hu, S.; Yang, C.; Li, Y.; Luo, Q.; Luo, H. *Biosens. Bioelectron.* **2022**, *199*, 113881.
(20) Liu, C.; You, X.; Lu, D.; Shi, G.; Deng, J.; Zhou, T. *ACS Appl. Bio. Mater.* **2020**, *3*, 7965−7973.
(21) Shen, Y.; Huang, Y.; Zhang, P.; Guo, B.; Jiang, H.; Tan, C.; Jiang, Y. *ACS Appl. Bio. Mater.* **2020**, *3*, 5639−5643.
(22) Zhang, H.; Wang, B.; Seehafer, K.; Bunz, U. H. F. *Chem. - Eur. J.* **2020**, *26*, 7779−7782.
(23) Fanni, A. M.; Monge, F. A.; Lin, C. Y.; Thapa, A.; Bhaskar, K.; Whitten, D. G.; Chi, E. Y. *ACS Chem. Neurosci.* **2019**, *10*, 1813−1825.
(24) Stains, C. I.; Ghosh, I. *ACS Chem. Biol.* **2007**, *2*, 525−528.
(25) Ran, C.; Zhao, W.; Moir, R. D.; Moore, A. *PLoS One* **2011**, *6*, No. e19362.
(26) Jiang, D.; Rauda, I.; Han, S.; Chen, S.; Zhou, F. *Langmuir* **2012**, *28*, 12711−12721.
(27) Kumar, A.; Bullard, R. L.; Patel, P.; Paslay, L. C.; Singh, D.; Bienkiewicz, E. A.; Morgan, S. E.; Rangachari, V. *PLoS One* **2011**, *6*, No. e18759.
(28) Ladiwala, A. R.; Lin, J. C.; Bale, S. S.; Marcelino-Cruz, A. M.; Bhattacharya, M.; Dordick, J. S.; Tessier, P. M. *J. Biol. Chem.* **2010**, *285*, 24228−24237.
(29) Planchard, M. S.; Samel, M. A.; Kumar, A.; Rangachari, V. *ACS Chem. Neurosci.* **2012**, *3*, 900−908.
(30) Sharma, A. K.; Pavlova, S. T.; Kim, J.; Kim, J.; Mirica, L. M. *Metallomics* **2013**, *5*, 1529−1536.
(31) Barghorn, S.; Nimmrich, V.; Striebinger, A.; Krantz, C.; Keller, P.; Janson, B.; Bahr, M.; Schmidt, M.; Bitner, R. S.; Harlan, J.; Barlow, E.; Ebert, U.; Hillen, H. *J. Neurochem.* **2005**, *95*, 834−847.

https://doi.org/10.1021/acs.analchem.2c00579
Anal. Chem. XXXX, XXX, XXX−XXX